HHS Public Access

Author manuscript

J Med Chem. Author manuscript; available in PMC 2016 April 09.

Published in final edited form as:

J Med Chem. 2015 April 9; 58(7): 3209–3222. doi:10.1021/acs.jmedchem.5b00155.

Design, Synthesis, in Vitro, and in Vivo Anticancer and Antiangiogenic Activity of Novel 3-Arylaminobenzofuran Derivatives Targeting the Colchicine Site on Tubulin

Romeo Romagnoli[*,†], **Pier Giovanni Baraldi**[*,†], **Maria Kimatrai Salvador**[†], **Filippo Prencipe**[†], **Carlota Lopez-Cara**[‡], **Santiago Schiaffino Ortega**[‡], **Andrea Brancale**[§], **Ernest Hamel**[‖], **Ignazio Castagliuolo**[#], **Stefania Mitola**[⊥], **Roberto Ronca**[⊥], **Roberta Bortolozzi**[∞], **Elena Porcù**[∞], **Giuseppe Basso**[∞], and **Giampietro Viola**[*,∞]

[†]Dipartimento di Scienze Farmaceutiche, Università di Ferrara, 44121 Ferrara, Italy

[‡]Departamento de Quimica Organica y Farmaceutica, Facultad de Farmacia, Universidad de Granada, Campus de Cartuja s/n, 18071, Granada, Spain

[§]School of Pharmacy and Pharmaceutical Sciences, Cardiff University, King Edward VII Avenue, Cardiff, CF10 3NB, U.K.

[‖]Screening Technologies Branch, Developmental Therapeutics Program, Division of Cancer Treatment and Diagnosis, Frederick National Laboratory for Cancer Research, National Cancer Institute, National Institutes of Health, Frederick, Maryland 21702, United States

[⊥]Dipartimento di Medicina Molecolare e Traslazionale, Unità di Oncologia Sperimentale ed Immunologia, Università di Brescia, 25121 Brescia, Italy

[#]Dipartimento di Medicina Molecolare, Università di Padova, 35121 Padova, Italy

[∞]Dipartimento di Salute della Donna e del Bambino, Laboratorio di Oncoematologia, Università di Padova, 35131 Padova, Italy

Abstract

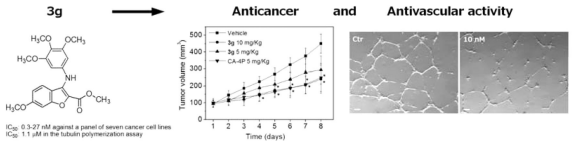

A new series of compounds characterized by the presence of a 2-methoxy/ethoxycarbonyl group, combined with either no substituent or a methoxy group at each of the four possible positions of the benzene portion of the 3-(3′,4′,5′-trimethoxyanilino)benzo[*b*]furan skeleton, were evaluated for antiproliferative activity against cancer cells in culture and, for selected, highly active

[*]**Corresponding Authors** R.R.: phone, 39-(0)532-455303; fax, 39-(0)532-455953; rmr@unife.it. P.G.B.: phone, 39-(0)532-455293; fax, 39-(0)532-455953; pgb@unife.it. G.V.: phone, 39-(0)49-8211451. fax, 39-(0)49-8211462; giampietro.viola1@unipd.it. .

Supporting Information HPLC traces and HRMS spectra of compounds **3g** and **3h**; molecular formula strings in csv format. This material is available free of charge via the Internet at http://pubs.acs.org.

The authors declare no competing financial interest.

compounds, inhibition of tubulin polymerization, cell cycle effects, and in vivo potency. The greatest antiproliferative activity occurred with a methoxy group introduced at the C-6 position, the least with this substituent at C-4. Thus far, the most promising compound in this series was 2-methoxycarbonyl-3-(3′,4′,5′-trimethoxyanilino)-6-methoxybenzo-[*b*]furan (3g), which inhibited cancer cell growth at nanomolar concentrations (IC_{50} values of 0.3–27 nM), bound to the colchicine site of tubulin, induced apoptosis, and showed, both in vitro and in vivo, potent vascular disrupting properties derived from the effect of this compound on vascular endothelial cells. Compound 3g had in vivo antitumor activity in a murine model comparable to the activity obtained with combretastatin A-4 phosphate.

INTRODUCTION

Microtubules, dynamic cellular structures in neoplastic and non-neoplastic cells, are generated by the polymerization of *α*,*β*-tubulin heterodimers.[1,2] Besides being critical for cell architecture, the microtubule system is essential for cell division, being the major component of the mitotic spindle, and for fundamental cellular processes, such as regulation of motility, cell signaling, secretion, and intracellular transport.[3–5] A significant number of antimitotic agents, many of which are natural products, interact specifically with tubulin and are able to affect tubulin polymerization.[6–8] More recent studies have demonstrated that several small molecules able to interfere with the dynamic assembly of tubulin in generating the microtubule system are also able to induce extensive morphological changes in the endothelial cells of tumor vasculature. Such agents can thus also be classified as vascular disrupting agents (VDAs).[9–12] The *cis*-stilbene natural product combretastatin A-4 (CA-4, 1, Chart 1), isolated by Pettit et al. from the bark of the South African bush willow tree *Combretum caffrum*,[13] strongly inhibits tubulin polymerization through binding to the colchicine site of tubulin.[14] CA-4 shows strong growth inhibition against a variety of cancer cells, including multidrug resistant cancer cell lines.[15] A water-soluble disodium phosphate ester derivative of **1a** (named CA-4P, **1b**) has shown promising results in clinical trials.[16] CA-4P is under evaluation in phase III trials for the treatment of anaplastic thyroid cancer and in phase II trials for non-small-cell lung cancer and platinum-resistant ovarian cancer.[17,18]

Previous studies have yielded a series of chemically diverse small molecules based on the benzo[*b*]furan scaffold, and the most active of these compounds act as antimitotic agents.[19–21] The 3-(3′,4′,5′-trimethoxybenzoyl)-6-methoxybenzo[*b*]furan molecular skeleton was the core structure of a series of antitubulin agents with general structure **2** identified by Pinney and co-workers as potent inhibitors of both tubulin polymerization and cell proliferation of the MCF-7 and MDA-MB-231 cancer cell lines.[22–24] While at the C-2 position there was a wide tolerance to structural variation with hydrophobic and hydrophilic substituents, at the C-3 position the carbon linker with the 3′,4′,5′-trimethoxyphenyl substituent was more effective as a carbonyl group than as a carbinol or a simple methylene group.[22] Previous studies have shown that the concomitant presence of a C-6 methoxy substituent significantly contributed to maximal activity, presumably as a mimic of the 4-methoxy group in the B-ring of CA-4.[23] The introduction of a hydroxyl at the C-7 position was well tolerated and afforded compounds with similar potency for R_2 = H, while a 10-fold

increase in activity was observed for R_2 = OH. Among the synthesized compounds, the C-2 methoxycarbonyl analogue **2a** showed potent activity in inhibiting the growth of the MDA-MB-231 human breast cancer cell line (IC_{50}: 1–10 nM). Moreover, **2a** had no significant selectivity against activated over quiescent human umbilical vein endothelial cells (HUVECs) (IC_{50}: 1–10 nM).[25] These findings prompted us to analyze this class of compounds in more detail. Specifically, we were intrigued by the idea of studying the biological effects of replacing the carbonyl group at the C-3 position of compound **2a** by an anilinic nitrogen (NH) moiety with hydrogen-bond accepting and donating capability to furnish a new series of 2-methoxy/ethoxycarbonyl-3-(3′,4′,5′-trimethoxyanilino)benzo[*b*]furan derivatives with general structure **3.** By the synthesis of this series of compounds, we focused on the effects on antiproliferative activity obtained by the insertion of an electron-donating methoxy substituent at the C-4, C-5, C-6, or C-7 positions, combined with the methoxy/ethoxycarbonyl substitution at the C-2 position of the benzo[*b*]furan nucleus. In this new class of compounds, the anilinic hydrogen at the C-3 position was also potentially able to generate an internal hydrogen bond with the sp_2-oxygen of the alkoxycarbonyl moiety.

CHEMISTRY

Compounds **3a–l** were synthesized by a two-step procedure described in Scheme 1. The condensation of 2-hydroxy-benzonitrile derivatives **4a–f**[21]with methyl or ethyl bromoacetate and K_2CO_3 in DMF furnished by a tandem “one-pot” cyclization procedure the 2-methoxy/ethoxycarbonyl-3-amino-benzo[*b*]furan derivatives **5a–l** in good yields. Finally, the novel derivatives **3a–l** were prepared using the C–N Buchwald–Hartwig palladium catalyzed cross-coupling protocol, by reaction of deactivated 3-amino benzo[*b*]furan analogues **5a–l** with 1-bromo-3,4,5-trimethoxybenzene in the presence of $Pd(OAc)_2$, *rac*-BINAP, and Cs_2CO_3 (as catalyst, ligand, and base, respectively) in toluene at 100 °C.

BIOLOGICAL RESULTS AND DISCUSSION

In Vitro Antiproliferative Activities. In Table 1 are summarized the in vitro antiproliferative activities of 2-methoxy/ethoxycarbonyl-3-(3′,4′,5′-trimethoxyanilino)benzo[*b*]furan derivatives **3a–l** against a panel of seven human cancer cell lines, using **1a** as reference compound. The results presented in Table 1 indicate that inhibition of cell growth was highly dependent upon the presence and position of the methoxy substituent on the benzene portion of the benzo[*b*]furan system. In both series of 2-alkoxycabonyl derivatives, the greatest activity occurred when the methoxy group was located at the C-6 position (**3g** and **3h**), the least when it was located at the C-4 (IC_{50} > 10 μM) position. In fact, the IC_{50} values obtained in the seven cell lines with the C-6 substituted compounds ranged from 0.3 to 27 (average, 7.8) nM with **3g** and from 13 to 100 (average, 34) nM with **3h**. The superiority of the methoxycarbonyl substituent over the ethoxycarbonyl substituent was observed in all of the cell lines except the MCF-7 cells, which were equally sensitive to both compounds. Overall, compounds **3i** (average IC_{50}, 370 nM) and **3j** (average IC_{50}, 670 nM), with the C-7 methoxy substituent, were more active than **3e** (average IC_{50}, 1500 nM) and **3f** (average IC_{50}, 2900 nM), with the C-5 methoxy substituent. For these latter two pairs of compounds, an occasional cell line was highly sensitive: RS 4;11 cells had IC_{50} values of 39 nM with **3e**

and 1 nM with **3i**, and Jurkat cells had an IC_{50} value of 30 nM with **3i**. Average IC_{50} values for the compounds bearing no methoxy substituent were 3300 and 2600 nM for compounds **3a** and **3b**, respectively. Thus, even the C-5 methoxy substituent improved overall compound activity. Finally, we also prepared both the methoxy- and ethoxycarbonyl compounds with a C-7 ethoxy substituent (**3k** and **3l**, respectively). With all cell lines, the C-7-ethoxy compound was significantly less active than its cognate C-7-methoxy compound.

The most potent compound identified in this study was the 2-methoxycarbonyl-3-(3′,4′,5′-trimethoxyanilino)-6-methoxybenzo[*b*]furan derivative **3g**, which was more active than the reference compound CA-4 in five of the seven cancer cell lines, while the two compounds had similar activity against Jurkat and HL-60 cells. The antiproliferative data obtained with **3g** may indicate that an anilinic nitrogen with a hydrogen as a proton bonding donor at the C-3 position of the benzo[b]furan skeleton can be a good surrogate for the carbonyl group in compounds with general structure **2**.

In a comparison of the two series of 2-alkoxycarbonyl derivatives with the methoxy group at the same position of the benzo[*b*]furan nucleus, the 2-methoxycarbonyl derivative generally had greater activity than its ethoxycarbonyl counterpart (i.e., **3e** vs **3f**, **3g** vs **3h**, **3i** vs **3j**, **3k** vs **3l**).

Evaluation of Antiproliferative Activity in Noncancer Cells

We investigated the effects of the two most active compounds (**3g** and **3h**) on noncancer cells. We examined human peripheral blood lymphocytes (PBLs) and HUVECs isolated from healthy donors. As shown in Table 2, in both unstimulated and mitogen-activated lymphocytes, the two compounds had little toxicity as compared to tumor cells. Somewhat greater toxicity was noted in HUVECs incubated with the two compounds, although also in this case the IC_{50} values were substantially higher than those obtained with the tumor cells. Moreover, in contrast to what was found with the tumor cells, **3h** was more active than **3g** in the noncancer cells. These results suggest that **3g** and **3h** may have a preferential selectivity toward cancer cells.

Inhibition of Tubulin Polymerization and Colchicine Binding

Compounds **3e** and **3g–j** and the reference compound CA-4 were evaluated for inhibitory effects on tubulin polymerization and on the binding of [^{3}H]colchicine to tubulin for an indication of whether their antiproliferative effects might be caused by an interaction with microtubules (Table 3).[26–28] The most potent of the compounds examined was **3g**, with an assembly IC_{50} of 1.1 μM, the same value obtained with CA-4, while **3h** was slightly less active than CA-4. This is in agreement with **3g** being the compound with the greatest antiproliferative activity. Compounds **3e**, **3i**, and **3j** were 6- to 7-fold less active than CA-4, with IC_{50} values of 7.5, 7.6, and 6.4 μM, respectively, which were consistent with their lower antiproliferative activity.

Colchicine binding studies were performed on the only derivatives (**3g** and **3h**) with tubulin assembly IC_{50} values lower than 5 μM. In reaction mixtures containing 1.0 μM tubulin and

5.0 μM [^{3}H]colchicine, compound **3g** potently inhibited the binding to [^{3}H]colchicine to tubulin, with 83% inhibition occurring when **3g** and radiolabeled drug were at 5.0 μM in the reaction mixture. Compound **3g** was less potent than **1a**, which in these experiments inhibited colchicine binding by 99%. Derivative **3h** was slightly less potent than **3g**, with 74% inhibition occurring with the compound at 5.0 μM.

For the most active compounds **3g** and **3h**, a good correlation was observed between antiproliferative activities and inhibition of tubulin polymerization and colchicine binding. These results suggest that these two derivatives act as microtubule-depolymerizing agents through an interaction with tubulin at the colchicine site or a site that overlaps the colchicine site.

Molecular Modeling

In order to investigate the possible binding mode of these novel compounds, a series of molecular docking studies were performed in the colchicine site of tubulin. In the binding mode for compound **3g** presented in Figure 1, the trimethoxyphenyl ring of the compound is in proximity to Cys241. Furthermore, there is a potential hydrogen bond between the ester moiety and Ala250, an interaction observed with other colchicine site agents.[29] These results could provide an explanation for the difference in biological activity observed for the compounds bearing a substituent in position 4, 5, or 7 of the benzo[*b*[furan (e.g., **3c**, **3e**, and **3i**) versus **3g** with its 6-methoxy group. Our models indicate that the colchicine-binding pocket cannot readily accommodate the compounds with the 4-, 5-, or 7-methoxy substituents.

Analysis of Cell Cycle Effects

The effects of a 24 h treatment with different concentrations of **3g** or **3h** on cell cycle progression were determined by flow cytometry in Jurkat and HeLa cells (Figure 2, panels A and B). The two compounds caused a significant G2/M arrest in a concentration-dependent manner in the cell lines tested, with a rise in G2/M cells occurring at a concentration as low as 60 nM, while at higher concentrations more than 70% of the cells were arrested in G2/M. The cell cycle arrest in G2/M phase was accompanied by a comparable reduction in the proportion of cells in both the G1 and S phases of the cell cycle.

We next studied the association between the induced G2/M arrest by the two compounds and alterations in expression of various proteins that regulate cell division. As shown in Figure 2 (panel C) in HeLa cells, a 24 h treatment with either compound at 100 or 250 nM caused a significant increase in cyclin B expression, which in association with cdc2 controls both entry into and exit from mitosis.[30,31] After a 48 h treatment, cyclin B expression decreased. More importantly, p-cdc2^{Tyr15} expression increased after a 24 h treatment, while at 48 h a slight decrease was observed. However, no major changes in the expression of phosphatase cdc25c were observed. These results indicate that arrest at G2/M induced by the compounds is caused by an increase of cyclin B activity, followed by its accumulation, leading to a decrease of p-cdc2^{Tyr15}. The decline in the level of p-cdc2^{Tyr15} at 48 h was more marked at the highest concentration (250 nM) examined.

Compounds 3g and 3h Induce Apoptosis through the Mitochondrial Pathway

The mode of cell death induced by **3g** and **3h** was investigated with the annexin-V assay.[32] As depicted in Figure 3 (panels A and B), HeLa cells treated with **3g** or **3h** for 24 or 48 h showed an accumulation of annexin-V positive cells in comparison with the control, in a concentration and time-dependent manner, and this is indicative of the occurrence of apoptosis.

Since many antimitotic compounds induce apoptosis through the mitochondrial pathway,[33–36] we determined whether **3g** and **3h** induced an alteration of the mitochondrial transmembrane potential ($\Delta\psi_{mt}$). $\Delta\psi_{mt}$ was monitored by flow cytometry using the dye 5,5′,6,6′-tetrachloro-1,1′,3,3′-tetraethylbenzimidazolcarbocyanine (JC-1). As shown in Figure 4 (panel A) in HeLa cells, both *3g* and *3h* induced a time- and concentration-dependent increase in the proportion of cells with depolarized mitochondria.

Mitochondrial membrane depolarization is associated with mitochondrial production of reactive oxygen species (ROS).[37] Therefore, we investigated whether ROS production increased after treatment with the test compounds. We measured the production of ROS by flow cytometry utilizing 2,7-dichlorodihydrofluorescein diacetate (H_2-DCFDA).

As shown in Figure 4 (panel B), both **3g** and **3h** induced the production of significant amounts of ROS in comparison with control cells, in agreement with the dissipation of $\Delta\psi_{mt}$. Altogether, these results indicate that these compounds induced apoptosis through the mitochondrial pathway.

Compounds 3g and 3h Induce Activation of Caspases and Down-Regulation of the Antiapoptotic Proteins Bcl-2 and Mcl-1

To determine whether compounds **3g** and **3h** induced caspase-dependent cell death, we performed an immunoblot analysis of the activation of caspase-9 and caspase-3, two caspases involved in the apoptotic mitochondrial pathway. Exposure of HeLa cells to either compound resulted in the activation of caspase-9 and caspase-3 in a time- and concentration-dependent manner, as shown in Figure 5. Moreover, we also observed the cleavage of poly(ADP-ribose) polymerase (PARP), which is one of the main cleavage targets of caspase-3, both in vitro and in vivo.[38]

Many recent studies have shown that regulation of the Bcl-2 family of proteins shares the signaling pathways induced by anti-microtubule compounds.[33,34] Several proapoptotic family proteins (e.g., Bax, Bid, Bim, and Bak) promote the release of cytochrome c, whereas antiapoptotic members (Bcl-2, Bcl-XL, and Mcl-1) are capable of antagonizing the proapoptotic proteins and preventing the loss of mitochondrial membrane potential. In agreement with these observations, we found that Bcl-2 after a 48 h treatment with either compound was reduced, while the expression of Mcl-1, which is another antiapoptotic member of the Bcl-2 family, was also strongly down-regulated. This change was observed after 48 h treatments at both 100 and 250 nM. However, at 24 h we observed an increase in the expression of Mcl-1 with **3g** but not with **3h**.

Altogether, our findings indicate that **3g** and **3h** are able to down-regulate the expression of antiapoptotic proteins in line with recent reports that suggest that sensitivity to antimitotic drugs is regulated by Mcl-1 levels.[39]

Evaluation of Antitumor Activity of Compound 3g in Vivo

To determine the in vivo antitumor activity of **3g**, a syngeneic hepatocellular carcinoma model in mice was used.[40] In preliminary experiments in vitro, we had determined that both compound **3g** and CA-4, used as reference compound, showed potent cytotoxic activity (**3g**, IC_{50} = 1.2 ± 0.6 nM; CA-4, IC_{50} = 0.9 ± 0.5 nM) against BNL 1ME A.7R.1 cells. Tumors were established by subcutaneous injection of BNL 1ME A.7R.1 cells into the backs of Balb/c mice. Once the tumor reached a measurable size (about 100 mm^3), 20 mice were randomly assigned to one of four groups. In two of the groups, compound **3g** was injected intraperitoneally at doses of 5 and 10 mg/kg, respectively. In a third group, CA-4P was injected at 5 mg/kg, while the fourth group was used as a control. As shown in Figure 6 (panel A), compound **3g** caused a significant reduction in tumor growth (44.5%), as compared with administration of vehicle, at the dose of 10 mg/kg but not at 5 mg/kg. At the lower dose the growth inhibition shown in the figure did not reach statistical significance. The effect of 5 mg/kg of CA-4P was not substantially different from that of 10 mg/kg of **3g**, and the CA-4P effect was significant relative to the control. During the treatment period, only a small decrease in body weight occurred in the animals treated with **3g** at the higher concentration (Figure 6, panel B).

Derivative 3g Has Antivascular Effects in Vitro and in Vivo

Recent antitumor strategies have included the use of chemotherapeutics with antiangiogenic or antivascular drugs to increase the efficacy of the treatment.[12] Many tubulin binding agents show antivascular effects against tumor endothelium,[12] including CA-4, and for that reason we evaluated **3g** for its effects on endothelial cells in vitro. We used HUVECs as a model to study angiogenesis in vitro. Endothelial cell migration to the tumor site is an important mechanism of angiogenesis,[41] and the inhibition of this process is a valuable strategy to arrest the development of tumor vasculature. With this aim, we evaluated endothelial cell motility by scratching a HUVEC monolayer and monitoring the ability of cells to reclose the wound. As shown in Figure 7 (panels A and B), **3g** was very efficient in arresting cell motility. The effect was statistically significant with only a 6 h incubation at 25 nM and became highly significant for all the tested concentrations after 24 h, even with only 5 nM **3g**.

To further evaluate the antivascular activity of **3g**, we analyzed the ability of the compound to disrupt the “tubule-like” structures formed by HUVECs seeded on Matrigel. Matrigel is an extracellular matrix rich in proangiogenic factors that stimulate single endothelial cells to assume an extended shape and produce a reticulum similar to a capillary network.

As shown in Figure 7 (panels C–E), after a 1 h (panels C and D) or 3 h (panel E) incubation, the compound clearly disrupted the network of HUVECs, as compared with the control. After 3 h, all the tested concentrations were effective in altering the tubule-like structures (Figure 7, panel C). Image analysis[42] was performed to obtain a quantitative measurement

of the total length of the tubules, the area and the number of meshes, the percent of area covered by HUVECs, and the number of branching points after both a 1 h (Figure 7, panel D) and 3 h (Figure 7, panel E) treatment. It is important to stress that **3g** exerted its antivascular effects in vitro at concentrations that did not affect HUVEC proliferation (see Table 2).

The antivascular activity of **3g** was also investigated in vivo. First, we used the chick embryo chorioallantoic membrane (CAM), which is a highly vascularized structure, as a model. Through alginate beads applied on the CAM, **3g** (1–100 pmol/egg) was slowly distributed within the membrane, starting from day 11 after egg fertilization, in the presence or absence of fibroblast growth factor (FGF) (100 ng/egg), a vascular growth factor. As shown in Figure 8 (panel A), **3g** alone, at the highest concentration (100 pmol/egg) used, did not induce blood vessels to increase in number. On the other hand, treatment with FGF gave rise to an extensive production of blood vessels, and this increase was strongly reduced by **3g** treatment, even at the lowest tested concentration (1 pmol/egg).

3g was further evaluated in a murine tumor model. BL6-B16 mouse melanoma cells, injected subcutaneously in syngeneic C57/BL6 mice, proliferate and generate tumor masses. After a 24 h treatment with **3g** at 30 mg/kg ip, the tumor was excised and the blood vessels were stained with an antibody against the endothelial marker CD31 and counted. As shown in Figure 8 (panel B), the number and, especially, the size of the vessels were reduced. This reduction in number was about 20% and was statistically significant (panel C, $P < 0.05$). Altogether our results indicate that **3g** is endowed with vascular disrupting properties both in vitro and in vivo. In addition, we also observed that the effects on endothelial cells induced by **3g** were similar to those observed after CA-4 treatment under the same experimental conditions, as described previously.[43]

CONCLUSIONS

We demonstrated that the bioisosteric replacement of the carbonyl bridge between the C-3 position of the benzo[*b*]furan ring and the 3,4,5-trimethoxyphenyl moiety by an anilinic nitrogen resulted in highly bioactive antimitotic agents based on the 2-alkoxycarbonyl-3-(3′,4′,5′-trimethoxyanilino)benzo[*b*]furan molecular skeleton. Compounds **3g** and **3h** were prepared by an efficient two-step synthetic procedure, and both compounds showed activity comparable with that of CA-4. Our structure–activity relationship studies involved placing the electron-donating methoxy substituent at the C-4, C-5, C-6, or C-7 position on the benzo[*b*]furan ring. For both the series of alkoxycarbonyl derivatives, compounds **3c** and **3d** with the methoxy group at the C-4 position were inactive, and a substantial improvement in antiproliferative activity occurred with the methoxy group at the C-5 position (**3e** and **3f**). Simply moving the methoxy group to C-6 resulted in the highly active compounds **3g** and **3h**, while moving the methoxy to C-7 (**3i** and **3j**) resulted in a drastic reduction in activity. The 2-methoxycarbonyl-3-(3′,4′,5′-trimethoxyanilino)-6-methoxybenzo[*b*]furan derivative **3g** had the greatest antiproliferative IC_{50} values, ranging from 0.3 to 27 nM against the seven cancer cell lines we examined. Compound **3g** was also a potent inhibitor of tubulin assembly, with an IC_{50} of 1.1 μM, similar to that of CA-4. Nevertheless, this compound was less active than CA-4 as an inhibitor of the binding of [^{3}H]colchicine to tubulin, with 83%

and 99% inhibition, respectively. Compound **3g**, in vitro was able to induce mitotic arrest followed by apoptosis through mitochondrial depolarization and activation of both caspase-9 and -3. Importantly, it exhibited significant antitumor activity in vivo and interesting antivascular properties. Thus, **3g** is a promising new tubulin binding agent with potential as an antitumor and antivascular agent that could improve common anticancer therapies.

EXPERIMENTAL SECTION

Chemistry. Materials and Methods

^{1}H NMR and ^{13}C NMR spectra were recorded in $CDCl_3$ solution with a Varian Mercury Plus 400 spectrometer at 400 and 100 MHz, respectively. Peak positions are given in parts per million (Δ) downfield from tetramethylsilane as internal standard, and *J* values are given in hertz. Positive-ion electrospray ionization (ESI) mass spectra were measured on a double-focusing Finnigan MAT 95 instrument with BE geometry. High resolution mass spectroscometry (HRMS) measurements were performed using an ESI-Q-TOF mass spectrometer (Agilent Technologies). Analytical HPLC analyses were performed at ambient temperature on a Beckman 125 liquid chromatograph fitted with a Luna C-18 column (4.6 mm × 100 mm, 3 μm particle size) with 0.1% TFA in H_2O (A) and 0.1% TFA in CH_3CN (B) solvent mixtures and equipped with a Beckman 168 diode array detector. Melting points (mp) were determined on a Buchi–Tottoli apparatus and are uncorrected. The purity of tested compounds was determined by combustion elemental analyses conducted by the Microanalytical Laboratory of the Chemistry Department of the University of Ferrara with a Yanagimoto MT-5 CHN recorder elemental analyzer. All tested compounds yielded data consistent with a purity of at least 95% as compared with the theoretical values. All reactions were carried out under an inert atmosphere of dry nitrogen, unless otherwise indicated. TLC was performed on silica gel (precoated F_{254} Merck plates), and compounds were visualized with aqueous $KMnO_4$. Flash column chromatography was performed using 230–400 mesh silica gel and the indicated solvent system. Organic solutions were dried over anhydrous Na_2SO_4. All commercial chemicals and solvents were reagent grade and were used without further treatment.

General Procedure A for the Synthesis of Compounds 5a–l

A suspension of the appropriate 2-hydroxybenzonitrile **4a–f** (5 mmol), methyl/ethyl bromoacetate (6 mmol, 1.2 equiv), and K_2CO_3 (1.38 g., 10 mmol, 2 equiv) in DMF (10 mL) was stirred at 60 °C for 4 h until consumption of the limiting reagent, followed by reflux heating for 8 h. The reaction mixture was cooled to ambient temperature and filtered through Celite. Then the filtrate was evaporated in vacuo. The residue was dissolved with ethyl acetate (30 mL), and the solution was washed sequentially with water (10 mL) and brine (10 mL). The organic layer was dried, filtered, and concentrated under reduced pressure, and the residue was purified by flash column chromatography on silica gel.

Methyl 3-Aminobenzofuran-2-carboxylate (5a)

Following general procedure A, the crude residue was purified by flash chromatography, using ethyl acetate/petroleum ether 2:8 (v:v) as eluent, to furnish **5a** as a yellow solid. Yield:

78%, mp 95–96 °C. ^{1}H NMR ($CDCl_3$) Δ: 3.97 (s, 3H), 4.99 (bs, 2H), 7.24 (m, 1H), 7.46 (m, 2H), 7.56 (dd, *J* = 7.8 and 1.0 Hz, 1H). MS (ESI): $[M]^+$ = 191.5.

Ethyl 3-Aminobenzofuran-2-carboxylate (5b)

Following general procedure A, the crude residue was purified by flash chromatography, using ethyl acetate/petroleum ether 2:8 (v:v) as eluent, to furnish **5b** as a green solid. Yield: 72%, mp 83–84 °C. ^{1}H NMR ($CDCl_3$) Δ: 1.40 (t, J = 7.2 Hz, 3H), 4.46 (q, *J* = 7:2 Hz, 2H), 4.97 (bs, 2H), 7.24 (m, 1H), 7.46 (m, 2H), 7.57 (dd, *J* = 7.8 and 1.0 Hz, 1H). MS (ESI): $[M + 1]^+$ = 206.1.

Methyl 3-Amino-4-methoxybenzofuran-2-carboxylate (5c)

Following general procedure A, the crude residue was purified by flash chromatography, using ethyl acetate/petroleum ether 3:7 (v:v) as eluent, to furnish **5c** as a white solid. Yield: 75%, mp 148–149 °C. ^{1}H NMR ($CDCl_3$) Δ: 3.94 (s, 3H), 3.96 (s, 3H), 5.40 (bs, 2H), 6.58 (d, *J* = 7.8 Hz, 1H), 6.99 (d, *J* = 8.4 Hz, 1H), 7.54 (t, *J* = 8.4 Hz, 1H). MS (ESI): $[M + 1]^+$ = 221.2.

Ethyl 3-Amino-4-methoxybenzofuran-2-carboxylate (5d)

Following general procedure A, the crude residue was purified by flash chromatography, using ethyl acetate/petroleum ether 3:7 (v:v) as eluent, to furnish **5d** as a colorless oil. Yield: 58%. ^{1}H NMR ($CDCl_3$) Δ: 1.42 (t, *J* = 7.2 Hz, 3H), 3.95 (s, 3H), 4.38 (q, *J* = 7.2 Hz, 2H), 5.42 (bs, 2H), 6.55 (d, *J* = 8.2 Hz, 1H), 7.04 (d, *J* = 8.6 Hz, 1H), 7.32 (t, *J* = 8.6 Hz, 1H). MS (ESI): $[M + 1]^+$ = 236.3.

Methyl 3-Amino-5-methoxybenzofuran-2-carboxylate (5e)

Following general procedure A, the crude residue was purified by flash chromatography, using ethyl acetate/petroleum ether 4:6 (v:v) as eluent, to furnish **5e** as a brown solid. Yield: 63%, mp 163–165 °C. ^{1}H NMR ($CDCl_3$) Δ: 3.86 (s, 3H), 3.96 (s, 3H), 4.90 (bs, 2H), 6.92 (d, *J* = 2.4 Hz, 1H), 7.06 (dd, *J* = 9.2 and 2.4 Hz, 1H), 7.61 (d, *J* = 9.2 Hz, 1H). MS (ESI): $[M + 1]^+$ = 222.2.

Ethyl 3-Amino-5-methoxybenzofuran-2-carboxylate (5f)

Following general procedure A, the crude residue was purified by flash chromatography, using ethyl acetate/petroleum ether 3:7 (v:v) as eluent, to furnish **5f** as a yellow solid. Yield: 53%, mp 151–153 °C. ^{1}H NMR ($CDCl_3$) Δ: 1.43 (t, *J* = 7.0 Hz, 3H), 3.86 (s, 3H), 4.45 (q, *J* = 7.0 Hz, 2H), 4.89 (bs, 2H), 6.92 (d, *J* = 2.4 Hz, 1H), 7.05 (dd, *J* = 9.0 and 2.4 Hz, 1H), 7.33 (d, *J* = 9.0 Hz, 1H). MS (ESI): $[M + 1]^+$ = 236.2.

Methyl 3-Amino-6-methoxybenzofuran-2-carboxylate (5g)

Following general procedure A, the crude residue was purified by flash chromatography, using ethyl acetate/petroleum ether 3:7 (v:v) as eluent, to furnish **5g** as a cream colored solid. Yield: 73%, mp 150–151 °C. ^{1}H NMR ($CDCl_3$) 3.84 (s, 3H), 3.94 (s, 3H), 4.97 (bs, 2H), 6.83 (dd, *J* = 8.6 and 2.2 Hz, 1H), 6.91 (d, *J* = 2.2 Hz, 1H), 7.39 (d, *J* = 8.6 Hz, 1H). MS (ESI): $[M + 1]^+$ = 222.1.

Ethyl 3-Amino-6-methoxybenzofuran-2-carboxylate (5h)

Following general procedure A, the crude residue was purified by flash chromatography, using ethyl acetate/petroleum ether 3:7 (v:v) as eluent, to furnish **5h** as a yellow solid. Yield: 52%, mp 145–147 °C. ^{1}H NMR (DMSO-d_6) 1.43 (t, J = 7.0 Hz, 3H), 3.85 (s, 3H), 4.40 (q, J = 7.0 Hz, 2H), 4.95 (bs, 2H), 6.85 (dd, J = 8.8 and 2.2 Hz, 1H), 6.93 (d, J = 2.2 Hz, 1H), 7.43 (d, J = 8.8 Hz, 1H). MS (ESI): $[M + 1]^+$ = 236.2.

Methyl 3-Amino-7-methoxybenzofuran-2-carboxylate (5i)

Following general procedure A, the crude residue was purified by flash chromatography, using ethyl acetate/petroleum ether 3:7 (v:v) as eluent, to furnish **5i** as a brown solid. Yield: 61%, mp 149–151 °C. ^{1}H NMR ($CDCl_3$) 3.94 (s, 3H), 3.98 (s, 3H), 4.96 (bs, 2H), 6.91 (dd, J = 7.0 and 2.0 Hz, 1H), 7.14 (m, 2H). MS (ESI): $[M + 1]^+$ = 222.1.

Ethyl 3-Amino-7-methoxybenzofuran-2-carboxylate (5j)

Following general procedure A, the crude residue was purified by flash chromatography, using ethyl acetate/petroleum ether 3:7 (v:v) as eluent, to furnish **5j** as a yellow solid. Yield: 78%, mp 123–125 °C. ^{1}H NMR ($CDCl_3$) 1.42 (t, J = 7.0 Hz, 3H), 3.99 (s, 3H), 4.40 (q, J = 7.0 Hz, 2H), 4.95 (bs, 2H), 6.90 (dd, J = 6.8 and 1.8 Hz, 1H), 7.13 (m, 2H). MS (ESI): $[M + 1]^+$ = 236.2.

Methyl 3-Amino-7-ethoxybenzofuran-2-carboxylate (5k)

Following general procedure A, the crude residue was purified by flash chromatography, using ethyl acetate/petroleum ether 3:7 (v:v) as eluent, to furnish **5k** as a yellow solid. Yield: 58%, mp 139–141 °C. ^{1}H NMR ($CDCl_3$) 1.50 (t, J = 7.2 Hz, 3H), 3.94 (s, 3H), 4.21 (q, J = 7.2 Hz, 2H), 4.95 (bs, 2H), 6.91 (dd, J = 6.8 and 2.2 Hz, 1H), 7.12 (m, 2H). MS (ESI): $[M + 1]^+$ = 236.3.

Ethyl 3-Amino-7-ethoxybenzofuran-2-carboxylate (5l)

Following general procedure A, the crude residue was purified by flash chromatography, using ethyl acetate/petroleum ether 3:7 (v:v) as eluent, to furnish **5l** as a yellow solid. Yield: 62%, mp 112–114 °C. ^{1}H NMR ($CDCl_3$) 1.42 (t, J = 7.2 Hz, 3H), 1.51 (t, J = 7.0 Hz, 3H), 4.26 (q, J = 7.2 Hz, 2H), 4.41 (q, J = 7.0 Hz, 2H), 4.93 (bs, 2H), 6.94 (dd, J = 7.0 and 2.2 Hz, 1H), 7.12 (m, 2H). MS (ESI): $[M + 1]^+$ = 250.3.

General Procedure B for the Preparation of Compounds 3a–l

To a dry Schlenk tube, dry toluene (5 mL), 3-aminobenzofuran derivative **5a–l** (0.5 mmol), $Pd(OAc)_2$ (6 mol %, 30 mg), *rac*-BINAP (4 mol %, 30 mg), $CsCO_3$ (230 mg, 0.7 mmol, 1.4 equiv), and 5-bromo-1,2,3-trimethoxybenzene (148 mg, 0.6 mmol, 1.2 equiv) were added under Ar, and the mixture was heated with stirring at 120 °C for 18 h. Upon cooling, ethyl acetate was added (5 mL), the mixture was filtered through Celite under vacuum and the filtrate diluted with ethyl acetate (10 mL) and water (5 mL). The aqueous phase was separated and further extracted with ethyl acetate (2 × 5 mL). The combined organic phases were washed with brine (5 mL), dried, concentrated under reduced pressure, and yielded a residue that was purified by flash column chromatography on silica gel.

Methyl 3-[(3,4,5-Trimethoxyphenyl)amino]benzofuran-2-carboxylate (3a)

Following general procedure B, the crude residue was purified by flash chromatography, using ethyl acetate/petroleum ether 2:8 (v:v) as eluent, to furnish **3a** as a yellow solid. Yield: 67%, mp 176–178 °C. ^{1}H NMR ($CDCl_3$) *δ*: 3.77 (s, 6H), 3.87 (s, 3H), 4.00 (s, 3H), 6.42 (s, 2H), 7.05 (m, 1H), 7.34 (d, *J* = 7.8 Hz, 1H), 7.48 (m, 2H), 7.74 (s, 1H). ^{13}C NMR ($CDCl_3$) *δ*: 51.9, 56.2 (2×), 61.2, 99.6 (2×), 112.8, 117.8, 120.9, 122.1, 123.6, 123.8, 128.8, 136.8, 137.1, 153.6 (2×), 154.6, 157.3. MS (ESI): $[M + 1]^+$ = 357.9. Anal. ($C_{19}H_{19}NO_6$) C, H, N.

Ethyl 3-[(3,4,5-Trimethoxyphenyl)amino]benzofuran-2-carboxylate (3b)

Following general procedure B, the crude residue was purified by flash chromatography, using ethyl acetate/petroleum ether 3:7 (v:v) as eluent, to furnish **3b** as a yellow solid. Yield: 56%, mp 122–124 °C. ^{1}H NMR ($CDCl_3$) *δ*: 1.46 (t, *J* = 7.0 Hz, 3H), 3.77 (s, 6H), 3.86 (s, 3H), 4.45 (q, *J* = 7.0 Hz, 2H), 6.41 (s, 2H), 7.12 (m, 1H), 7.32 (d, *J* = 7.8 Hz, 1H), 7.54 (m, 2H), 7.80 (s, 1H). ^{13}C NMR ($CDCl_3$) *δ*: 14.6, 56.1 (2×), 60.8, 61.1, 99.4 (2×), 109.9, 112.8, 117.8, 120.9, 121.9, 123.5, 128.6, 136.5, 126.8, 153.5 (2×), 154.4, 158.1. MS (ESI): $[M + 1]^+$ = 372.4. Anal. ($C_{20}H_{21}NO_6$) C, H, N.

Methyl 3-(3,4,5-Trimethoxyphenylamino)-4-methoxybenzofuran-2-carboxylate (3c)

Following general procedure B, the crude residue was purified by flash chromatography, using ethyl acetate/petroleum ether 3:7 (v:v) as eluent, to furnish **3c** as a white solid. Yield: 63%, mp 171–172 °C. ^{1}H NMR ($CDCl_3$) *δ*: 3.66 (s, 6H), 3.78 (s, 3H), 3.84 (s, 3H), 3.91 (s, 3H), 6.38 (s, 2H), 7.02 (dd, *J* = 8.6 and 2.0 Hz, 1H), 7.32 (d, *J* = 2.0 Hz, 1H), 7.48 (d, *J* = 8.6 Hz, 1H), 7.77 (s, 1H). ^{13}C NMR ($CDCl_3$) *δ*: 51.8, 53.2, 56.8 (2×), 60.9, 99.6 (2×), 105.2, 105.9, 107.2, 119.4, 124.6, 127.7, 135.1, 135.8, 153.6 (2×), 155.8, 155.9, 163.3. MS (ESI): $[M + 1]^+$ = 388.2. Anal. ($C_{20}H_{21}NO_7$) C, H, N.

Ethyl 3-(3,4,5-Trimethoxyphenylamino)-4-methoxybenzofuran-2-carboxylate (3d)

Following general procedure B, the crude residue was purified by flash chromatography, using ethyl acetate/petroleum ether 3:7 (v:v) as eluent, to furnish **3d** as a yellow solid. Yield: 61%, mp 83–85 °C. ^{1}H NMR ($CDCl_3$) *δ*: 1.44 (t, *J* = 7.2 Hz, 3H), 3.68 (s, 6H), 3.76 (s, 3H), 3.94 (s, 3H), 4.32 (q, *J* = 7.2 Hz, 2H), 6.32 (s, 2H), 6.49 (d, *J* = 8.2 Hz, 1H), 6.95 (d, *J* = 8.6 Hz, 1H), 7.34 (t, *J* = 8.6 Hz, 1H), 7.77 (s, 1H). ^{13}C NMR ($CDCl_3$) *δ*: 14.4, 51.8, 53.3, 56.7 (2×), 99.6 (2×), 104.5, 105.2, 105.7, 107.0, 118.8, 124.5, 127.9, 135.0, 135.6, 153.8 (2×), 155.9, 160.0, 163.8. MS (ESI): $[M + 1]^+$ = 402.2. Anal. ($C_{21}H_{23}NO_7$) C, H, N.

Methyl 3-(3,4,5-Trimethoxyphenylamino)-5-methoxybenzofuran-2-carboxylate (3e)

Following general procedure B, the crude residue was purified by flash chromatography, using ethyl acetate/petroleum ether 3:7 (v:v) as eluent, to furnish **3e** as a yellow solid. Yield: 53% yield, mp 140–142 °C. ^{1}H NMR ($CDCl_3$) *δ*: 3.65 (s, 3H), 3.79 (s, 6H), 3.86 (s, 3H), 3.99 (s, 3H), 6.48 (s, 2H), 6.68 (d, *J* = 2.8 Hz, 1H), 7.07 (dd, *J* = 9.0 and 2.8 Hz, 1H), 7.42 (d, *J* = 9.0 Hz, 1H), 7.78 (s, 1H). ^{13}C NMR ($CDCl_3$) *δ*: 51.9, 55.9, 56.2 (2×), 61.2, 99.3 (2×), 104.5, 112.8, 113.5, 113.8, 116.5, 118.9, 132.2, 132.6, 135.8, 136.9, 153.6 (2×), 158.2. MS (ESI): $[M + 1]^+$ = 388.0. Anal. ($C_{20}H_{21}NO_7$) C, H, N.

Ethyl 3-(3,4,5-Trimethoxyphenylamino)-5-methoxybenzofuran-2-carboxylate (3f)

Following general procedure B, the crude residue was purified by flash chromatography, using ethyl acetate/petroleum ether 3:7 (v:v) as eluent, to furnish **3f** as a yellow solid. Yield: 56% yield, mp 105–107 °C. ^{1}H NMR ($CDCl_3$) *δ*: 1.46 (t, *J* = 7.0 Hz, 3H), 3.65 (s, 3H), 3.79 (s, 6H), 3.86 (s, 3H), 4.44 (q, *J* = 7.0 Hz, 2H), 6.40 (s, 2H), 6.69 (d, *J* = 2.8 Hz, 1H), 7.07 (dd, *J* = 9.2 and 2.8 Hz, 1H), 7.43 (d, *J* = 9.2 Hz, 1H), 7.70 (s, 1H). ^{13}C NMR ($CDCl_3$) *δ*: 14.7, 55.9, 55.2 (2×), 60.9, 61.2, 99.1 (2×), 104.5, 113.6, 118.8, 121.3, 128.9, 134.4, 136.4, 137.0, 149.6, 153.6 (2×), 154.9, 161.9. MS (ESI): $[M + 1]^+$ = 402.2. Anal. ($C_{21}H_{23}NO_7$) C, H, N.

Methyl 3-(3,4,5-Trimethoxyphenylamino)-6-methoxybenzofuran-2-carboxylate (3g)

Following general procedure B, the crude residue was purified by flash chromatography, using ethyl acetate/petroleum ether 3:7 (v:v) as eluent, to furnish **3g** as a yellow solid. Yield: 78%, mp 143–145 °C. ^{1}H NMR ($CDCl_3$) *δ*: 3.78 (s, 6H), 3.85 (s, 3H), 3.86 (s, 3H), 3.97 (s, 3H), 6.42 (s, 2H), 6.71 (dd, *J* = 8.8 and 1.8 Hz, 1H), 6.94 (d, *J* = 1.8 Hz, 1H), 7.18 (d, *J* = 8.8 Hz, 1H), 7.72 (s, 1H). ^{13}C NMR ($CDCl_3$) *δ*: 51.7, 55.7, 56.2 (2×), 61.2, 95.8, 99.7 (2×), 112.3, 114.1, 120.1, 124.1, 136.5, 136.9, 153.6 (2×), 155.8, 156.1, 160.3, 161.3. MS (ESI): $[M + 1]^+$ = 388.0. Anal. ($C_{20}H_{21}NO_7$) C, H, N. HRMS calculated for $C_{20}H_{21}NO_7$ $(M + H)^+$, 388.1391; found, 388.13909.

Ethyl 3-(3,4,5-Trimethoxyphenylamino)-6-methoxybenzofuran-2-carboxylate (3h)

Following general procedure B, the crude residue was purified by flash chromatography, using ethyl acetate/petroleum ether 3:7 (v:v) as eluent, to furnish **3h** as a yellow solid. Yield: 57%, mp 110–112 °C. ^{1}H NMR ($CDCl_3$) *δ*: 1.45 (t, *J* = 6.8 Hz, 3H), 3.78 (s, 6H), 3.80 (s, 3H), 3.86 (s, 3H), 4.43 (q, *J* = 6.8 Hz, 2H), 6.42 (s, 2H), 6.70 (dd, *J* = 8.8 and 2.2 Hz, 1H), 6.96 (d, *J* = 2.2 Hz, 1H), 7.19 (d, *J* = 8.8 Hz, 1H), 7.77 (s, 1H). ^{13}C NMR ($CDCl_3$) *δ*: 14.7, 55.7, 56.2 (2×), 60.7, 61.2, 95.9, 99.5 (2×), 112.2, 113.1, 124.0, 125.9, 127.7, 136.6, 140.0, 153.6 (2×), 154.01, 156.2, 161.2. MS (ESI): $[M + 1]^+$ = 402.2. Anal. ($C_{21}H_{23}NO_7$) C, H, N. HRMS calculated for $C_{21}H_{23}NO_7$ $(M + H)^+$, 402.1547; found, 402.1546.

Methyl 3-(3,4,5-Trimethoxyphenylamino)-7-methoxybenzofuran-2-carboxylate (3i)

Following general procedure B, the crude residue was purified by flash chromatography, using ethyl acetate/petroleum ether 3:7 (v:v) as eluent, to furnish **3i** as a yellow solid. Yield: 68%, mp 177–179 °C. ^{1}H NMR ($CDCl_3$) *δ*: 3.77 (s, 6H), 3.86 (s, 3H), 3.97 (s, 3H), 4.00 (s, 3H), 6.40 (s, 2H), 6.92 (m, 2H), 6.99 (m, 1H), 7.72 (s, 1H). ^{13}C NMR ($CDCl_3$) *δ*: 51.7, 55.9, 56.1 (2×), 61.2, 99.5 (2×), 109.4, 115.4, 121.0, 122.5, 122.7, 124.5, 136.8, 139.1, 146.2, 147.1, 153.6 (2×), 162.3. MS (ESI): $[M + 1]^+$ = 388.2. Anal. ($C_{20}H_{21}NO_7$) C, H, N.

Ethyl 3-(3,4,5-Trimethoxyphenylamino)-7-methoxybenzofuran-2-carboxylate (3j)

Following general procedure B, the crude residue was purified by flash chromatography, using ethyl acetate/petroleum ether 3:7 (v:v) as eluent, to furnish **3j** as a white solid. Yield: 73%, mp 184–186 °C. ^{1}H NMR ($CDCl_3$) *δ*: 1.47 (t, *J* = 7.0 Hz, 3H), 3.77 (s, 6H), 3.86 (s, 3H), 4.00 (s, 3H), 4.47 (q, *J* = 7.0 Hz, 2H), 6.40 (s, 2H), 6.91 (m, 2H), 6.99 (m, 1H), 7.78 (s, 1H). ^{13}C NMR ($CDCl_3$) *δ*: 14.7, 56.0, 56.1 (2×), 60.8, 61.2, 99.3 (2×), 106.5, 108.6, 109.3,

110.5, 115.4, 122.7, 124.5, 135.9, 137.0, 149.5, 153.6 (2×), 161.5. MS (ESI): $[M + 1]^+$ = 402.2. Anal. ($C_{21}H_{23}NO_7$) C, H, N.

Methyl 3-(3,4,5-Trimethoxyphenylamino)-7-ethoxybenzofuran-2-carboxylate (3k)

Following general procedure B, the crude residue was purified by flash chromatography, using ethyl acetate/petroleum ether 3:7 (v:v) as eluent, to furnish **3k** as a yellow solid. Yield: 73%, mp 135–137 °C. ^{1}H NMR ($CDCl_3$) δ: 1.52 (t, J = 7.0 Hz, 3H), 3.77 (s, 6H), 3.86 (s, 3H), 3.98 (s, 3H), 4.24 (q, J = 7.0 Hz, 2H), 6.40 (s, 2H), 6.88 (m, 2H), 6.97 (m, 1H), 7.71 (s, 1H). ^{13}C NMR ($CDCl_3$) δ: 14.8, 51.6, 56.0 (2×), 61.1, 64.5, 99.3 (2×), 109.2, 110.4, 115.1, 118.2, 122.4, 122.6, 134.5, 136.8, 144.6, 145.4, 153.5 (2×), 162.2. MS (ESI): $[M + 1]^+$ = 402.0. Anal. ($C_{21}H_{23}NO_7$) C, H, N.

Ethyl 3-(3,4,5-Trimethoxyphenylamino)-7-ethoxybenzofuran-2-carboxylate (3l)

Following general procedure B, the crude residue was purified by flash chromatography, using ethyl acetate/petroleum ether 3:7 (v:v) as eluent, to furnish **3l** as a yellow solid. Yield: 52%, mp 149–151 °C. ^{1}H NMR ($CDCl_3$) δ: 1.41 (t, J = 7.2 Hz, 3H), 1.53 (t, J = 7.0 Hz, 3H), 3.77 (s, 6H), 3.85 (s, 3H), 4.24 (q, J = 7.2 Hz, 2H), 4.44 (q, J = 7.0 Hz, 2H), 6.40 (s, 2H), 6.90 (m, 2H), 6.97 (m, 1H), 7.75 (s, 1H). ^{13}C NMR ($CDCl_3$) δ: 14.6, 14.8, 56.0 (2×), 60.7, 61.1, 64.5, 99.21 (2×), 108.8, 110.4, 115.1, 122.6, 123.5, 133.9, 134.1, 136.7, 136.9, 139.9, 153.5 (2×), 175.3. MS (ESI): $[M + 1]^+$ = 416.2. Anal. ($C_{22}H_{25}NO_7$) C, H, N.

Molecular Modeling

All molecular docking studies were performed on a MacPro dual 2.66 GHz Xeon running Ubuntu 12.04. The simulations were carried out using two tubulin structures (http://www.rcsb.org/, PDB code 1SA0,[44] PDB code 3HKC[45]). Hydrogen atoms were added to the protein, using the Protonate 3D routine of the Molecular Operating Environment (MOE).[46] Ligand structures were built with MOE and minimized using the MMFF94x force field until a rmsd gradient of 0.05 kcal mol^{-1} Å^{-1} was reached. The docking simulations were performed using PLANTS.[47] The docking results obtained using the two different protein structures were equivalent.

Antiproliferative Assays

Human T-cell leukemia (Jurkat), human B-cell leukemia (RS4;11), and human promyelocytic leukemia (HL-60) cells were grown in RPMI-1640 medium, (Gibco, Milano, Italy). Breast adenocarcinoma (MCF-7), human non-small-cell lung carcinoma (A549), human cervix carcinoma (HeLa), and human colon adenocarcinoma (HT-29) cells were grown in DMEM medium (Gibco, Milano, Italy). Both media were supplemented with 115 units/mL of penicillin G (Gibco, Milano, Italy), 115 μg/mL of streptomycin (Invitrogen, Milano, Italy), and 10% fetal bovine serum (Invitrogen, Milano, Italy). These cell lines were purchased from ATCC. Stock solutions (10 mM) of the different compounds were obtained by dissolving them in dimethyl sulfoxide (DMSO). Individual wells of a 96-well tissue culture microtiter plate were inoculated with 100 μL of complete medium containing 8×10^3 cells. The plates were incubated at 37 °C in a humidified 5% CO_2 incubator for 18 h prior to the experiments. After medium removal, 100 μL of fresh medium containing the test

compound at different concentrations was added to each well and incubated at 37 °C for 72 h. The percentage of DMSO in the medium never exceeded 0.25%. This was also the maximum DMSO concentration in all cell-based assays described below. Cell viability was assayed by the (3-(4,5-dimethylthiazol-2-yl)-2,5-diphenyltetrazolium bromide test as previously described.[36] The IC_{50} was defined as the compound concentration required to inhibit cell proliferation by 50%, in comparison with cells treated with the maximum amount of DMSO, which was considered 100% viability.

PBLs from healthy donors were obtained by separation on Lymphoprep (Fresenius KABI Norge AS) gradient. After extensive washing, cells were resuspended (1.0×10^6 cells/mL) in RPMI-1640 with 10% fetal bovine serum and incubated overnight. For cytotoxicity evaluations in proliferating PBL cultures, nonadherent cells were resuspended at 5×10^5 cells/mL in growth medium containing 2.5 μg/mL PHA (Irvine Scientific). Different concentrations of the test compounds were added, and viability was determined 72 h later by the MTT test. For cytotoxicity evaluations in resting PBL cultures, nonadherent cells were resuspended (5×10^5 cells/mL) and treated for 72 h with the test compounds, as described above.

Effects on Tubulin Polymerization and on Colchicine Binding to Tubulin

To evaluate the effect of the compounds on tubulin assembly in vitro,[26] varying concentrations of compounds were preincubated with 10 μM bovine brain tubulin in glutamate buffer at 30 °C and then cooled to 0 °C. After addition of 0.4 mM GTP (final concentration), the mixtures were transferred to 0 °C cuvettes in a recording spectrophotometer and warmed to 30 °C. Tubulin assembly was followed turbidimetrically at 350 nm. The IC_{50} was defined as the compound concentration that inhibited the extent of assembly by 50% after a 20 min incubation. The ability of the test compounds to inhibit colchicine binding to tubulin was measured as described[28] except that the reaction mixtures contained 1 μM tubulin, 5 μM [^{3}H]colchicine, and 5 μM test compound.

Flow Cytometric Analysis of Cell Cycle Distribution

5×10^5 HeLa or Jurkat cells were treated with different concentrations of the test compounds for 24 h. After the incubation period, the cells were collected, centrifuged, and fixed with ice-cold ethanol (70%). The cells were then treated with lysis buffer containing RNase A and 0.1% Triton X-100 and then stained with propidium iodide (PI). Samples were analyzed on a Cytomic FC500 flow cytometer (Beckman Coulter). DNA histograms were analyzed using MultiCycle for Windows (Phoenix Flow Systems).

Apoptosis Assay

Cell death was determined by flow cytometry of cells double stained with annexin V/FITC and PI. The Coulter Cytomics FC500 (Beckman Coulter) was used to measure the surface exposure of phosphatidylserine on apoptotic cells according to the manufacturer's instructions (Annexin-V Fluos, Roche Diagnostics).

Assessment of Mitochondrial Changes

The mitochondrial membrane potential was measured with the lipophilic cationic dye JC-1 (Molecular Probes), as described.[48] The production of ROS was measured by flow cytometry using H_2DCFDA (Molecular Probes), as previously described.[48]

Western Blot Analysis

HeLa cells were incubated in the presence of **3g** or **3h** and, after different times, were collected, centrifuged, and washed two times with ice cold phosphate buffered saline (PBS). The pellet was then resuspended in lysis buffer. After the cells were lysed on ice for 30 min, lysates were centrifuged at 15000*g* at 4 °C for 10 min. The protein concentration in the supernatant was determined using the BCA protein assay reagents (Pierce, Italy). Equal amounts of protein (10 μg) were resolved using sodium dodecyl sulfate–polyacrylamide gel electrophoresis (7.5–15% acrylamide gels) and transferred to PVDF Hybond-P membrane (GE Healthcare). Membranes were blocked with a 5% bovine serum albumin solution in Tween PBS, the membranes being gently rotated overnight at 4 °C. Membranes were then incubated with primary antibodies against Bcl-2, PARP, cleaved caspase-9, cdc25c (Cell Signaling), caspase-3 (Alexis), H2AX (Cell Signaling), p53 (Cell Signaling), cyclin B (Cell Signaling), p-cdc2^{Tyr15} (Cell Signaling), Mcl-1 (Cell Signaling), or β-actin (Sigma-Aldrich) for 2 h at room temperature. Membranes were next incubated with peroxidase labeled secondary antibodies for 60 min. All membranes were visualized using ECL Select (GE Healthcare) and exposed to Hyperfilm MP (GE Healthcare). To confirm equal protein loading, each membrane was stripped and reprobed with anti-β-actin antibody.

Evaluation of Antivascular Activity in Vitro

HUVECs were prepared from human umbilical cord veins, as previously described.[43] The adherent cells were maintained in M200 medium supplemented with low serum growth supplement, containing fetal bovine serum, hydrocortisone, hEGF, bFGF, heparin, gentamycin/amphotericin (Life Technologies, Monza, Italy). Once confluent, the cells were detached by treatment with a trypsin–EDTA solution and used in experiments from the first to sixth passages.

The motility assay for HUVECs was based on “scratch” wounding of a confluent monolayer.[49] Briefly, HUVECs (1×10^5) were seeded onto 0.1% collagen type I (BD Biosciences, Italy) coated six-well plates in complete medium until a confluent monolayer was formed. The cells were wound using a pipet tip, and wells were washed with PBS to remove the detached cells. Then the cells were treated with the test compounds, and at different times from scratch, the cells were photographed under a light microscope. At all indicated time points, the wound width was measured in four areas and compared with the initial width.

Matrigel matrix (Basement Membrane Matrix, BD Biosciences, Italy) was kept at 4 °C for 3 h, when 230 μL of Matrigel solution was added to each well of a 24-well plate. After gelling at 37 °C for 30 min, gels were overlaid with 500 μL of medium containing 6×10^4 HUVECs. The cells were incubated over Matrigel for 6 h to allow capillary tubes to form. Different concentrations of test compound were added in the cultures and incubated for

different times, and the disappearance of existing vasculature was monitored and photographed (five fields for each well: the four quadrants and the center) at 10× magnification. Phase contrast images were recorded using a digital camera and saved as TIFF files. Image analysis was carried out using ImageJ image analysis software, and the following dimensional parameters (percent area covered by HUVECs and total length of HUVECs network per field) and topological parameters (number of meshes and branching points per field) were estimated.[42] Values were expressed as percent change from control cultures grown with complete medium.

In Vivo CAM Assay in Fertilized Chicken Eggs

Alginate pellets containing 0.1–1.0 pmol per pellet of TR-644 or CA4 were grafted on the CAM of fertilized chicken eggs at day 11. After 72 h, new blood vessels converging toward the implant were counted at 5× magnification under a stereomicroscope.

Antivascular Activity in Vivo

Six week old C57BL/6 mice (Charles River, Calco, Italy) were injected subcutaneously into the dorsolateral flank with 10^5 BL6-B16 murine melanoma cells in 200 μL of PBS. When tumor volume reached 300 mm^3, animals were treated intraperitoneally with **3g** (30 mg/kg) dissolved in DMSO (50 μL). Twenty-four hours later, tumors were harvested, embedded in OCT compound (Bio-Optica), and immediately frozen in liquid nitrogen for immunohistochemical analysis, as previously described.[43] Excised tumors were cut with a cryostat into 4–5 μm sections. Immunohistochemistry was performed by staining samples with rat anti-mouse CD31 antibody (1:200; BD Biosciences) and biotinylated goat anti-rat secondary antibody (1:100; BD Biosciences). Quantification was performed by counting the number of CD31 positive vessels in 5 fields per section, using a 40× objective.

Antitumor Activity in Vivo

The in vivo cytotoxic activity of compound **3g** was investigated using a syngeneic murine hepatocellular carcinoma cell line (BNL 1ME A.7R.1) in Balb/c mice.[40] Male mice, 8 weeks old, were purchased from Harlan (S. Pietro al Natisone Udine, Italy), and tumors were induced by a subcutaneous injection in their dorsal region of 10^7 cells in 200 μL of sterile PBS. Animals were randomly divided into four groups, and starting on the second day, the first group was daily dosed intraperitoneally with 7 μL/g of vehicle (0.9% NaCl containing 5% polyethylene glycol 400 and 0.5% Tween 80). Groups 2 and 3 were treated with compound **3g** at the doses of 5 or 10 mg/kg body weight, respectively. The fourth group received the reference compound CA-4P at 5 mg/kg body weight. Both compound **3g** and CA-4P were dissolved in vehicle. Tumor sizes were measured daily for 7 days using a pair of calipers. Tumor volume (V) was calculated by the rotational ellipsoid formula: $V = AB^2/2$, where A is the longer diameter (axial) and B is the shorter diameter (rotational). All experimental procedures followed guidelines recommended by the Institutional Animal Care and Use Committee of Padova University.

Statistical Analysis

Unless indicated otherwise, results are presented as the mean ± SEM. The differences between different treatments were analyzed using the two-sided Student's *t* test. *P* values less than 0.05 were considered significant.

Supplementary Material

Refer to Web version on PubMed Central for supplementary material.

ACKNOWLEDGMENTS

The research was supported by PRIN 2010–2011 (Grant 2010W7YRLZ_007) and "Consejería de Economía, Innovación, Ciencia y Empleo, Junta de Andalucia" (Grant P12-CTS-696). The authors thank Dr. Alberto Casolari for excellent technical assistance.

ABBREVIATIONS USED

CA-4	combretastatin A-4
CA-4P	combretastatin A-4 phosphate
DMF	*N*,*N*-dimethylformamide
$Pd(OAc)_2$	palladium(II) acetate
BINAP	*rac*-2,2′-bis(diphenylphosphane)-1,1′-binaphthyl
PBL	peripheral blood lymphocyte
PHA	phytohemaglutinin
FITC	fluorescein isothiocyanate
PI	propidium iodide
FGF	fibroblast growth factor
$\Delta\psi_{mt}$	mitochondrial transmembrane potential
JC-1	5,5′,6,6′-tetrachloro-1,1′,3,3′-tetraethylbenzimidazolcarbocyanine
ROS	reactive oxygen species
H_2DCFDA	2,7-dichlorodihydrofluorescein diacetate
PARP	poly(ADP-ribose) polymerase
DMSO	dimethyl sulfoxide
PBS	phosphate-buffered saline
TFA	trifluoroacetic acid

REFERENCES

(1). Aylett, CHS.; Löwe, J.; Amos, LA. New insights into the mechanisms of cytomotive actin and tubulin filaments. In: Jeon, KW., editor. International Review of Cell and Molecular Biology. Vol. Vol. 292. Academic Press; Burlington, MA: 2011. p. 1-71.

(2). Kueh HY, Mitchison TJ. Structural plasticity in actin and tubulin polymer dynamics. Science. 2009; 325:960–963. [PubMed: 19696342]

(3). Sorger PK, Dobles M, Tournebize R, Hyman AA. Coupling cell division and cell death to microtubule dynamics. Curr. Opin. Cell. Biol. 1997; 9:807–814. [PubMed: 9425345]

(4). Downing KH, Nogales E. Tubulin structure: insights into microtubule properties and functions. Curr. Opin. Struct. Biol. 1998; 8:785–791. [PubMed: 9914260]

(5). McIntosh JR, Grishchuk E, West RR. Chromosome-microtubule interactions during mitosis. Annu. Rev. Cell Dev. Biol. 2002; 18:193–219. [PubMed: 12142285]

(6). Honore S, Pasquier E, Braguer D. Understanding microtubule dynamics for improved cancer therapy. Cell. Mol. Life Sci. 2005; 62:3039–3056. [PubMed: 16314924]

(7). Chen S-M, Meng L-H, Ding J. New microtubule-inhibiting anticancer agents. Expert Opin. Invest. Drugs. 2010; 3:329–343.

(8). Amos LA. What tubulin drugs tell us about microtubule structure and dynamics. Semin. Cell Dev. Biol. 2011; 22:916–926. [PubMed: 22001382]

(9). Kanthou C, Tozer GM. Microtubule depolymerizing vascular disrupting agents: novel therapeutic agents for oncology and other pathologies. Int. J. Exp. Pathol. 2009; 90:284–294. [PubMed: 19563611]

(10). Porcù E, Bortolozzi R, Basso G, Viola G. Recent advances on vascular disrupting agents. Future Med. Chem. 2014; 6:1485–1498. [PubMed: 25365233]

(11). Mason RP, Zhao D, Liu L, Trawick ML, Pinney KG. A perspective on vascular disrupting agents that interact with tubulin: preclinical tumor imaging and biological assessment. Integr. Biol. 2011; 3:375–387.

(12). Schwartz EL. Antivascular actions of microtubule-binding drugs. Clin. Cancer Res. 2009; 15:2594–2601. [PubMed: 19351751]

(13). Pettit GR, Singh SB, Hamel E, Lin CM, Alberts DS, Garcia-Kendall D. Isolation and structure of the strong cell growth and tubulin inhibitor combretastatin A-4. Experentia. 1989; 45:209–211.

(14). Lin CM, Ho HH, Pettit GR, Hamel E. Antimitotic natural products combretastatin A-4 and combretastatin A-2: studies on the mechanism of their inhibition of the binding of colchicine to tubulin. Biochemistry. 1989; 28:6984–6991. [PubMed: 2819042]

(15). McGown AT, Fox BW. Differential cytotoxicity of combretastatins A1 and A4 in two daunobucin-resistant P388 cell lines. Cancer Chemother. Pharmacol. 1990; 26:79–81. [PubMed: 2322992]

(16). Siemann DW, Chaplin DJ, Walicke PA. A review and update of the current status of the vasculature-disabling agent combretastatin-A4 phosphate (CA4P). Expert Opin. Invest. Drugs. 2009; 18:189–197.

(17). Zweifel M, Jayson GC, Reed NS, Osborne R, Hassan B, Ledermann J, Shreeves G, Poupard L, Lu SP, Balkissoon J, Chaplin DJ, Rustin GJS. Phase II trial of combretastatin A4 phosphate, carboplatin, and paclitaxel in patients with platinum resistant ovarian cancer. Ann. Oncol. 2011; 22:2036–2041. [PubMed: 21273348]

(18). Rustin GJ, Shreeves G, Nathan PD, Gaya A, Ganesan TS, Wang D, Boxall J, Poupard L, Chaplin DJ, Stratford MRL, Balkissoon J, Zweifel MA. Phase Ib trial of CA4P (combretastatin A-4 phosphate), carboplatin, and paclitaxel in patients with advanced cancer. Br. J. Cancer. 2010; 102:1355–1360. [PubMed: 20389300]

(19). Kamal A, Reddy NVS, Nayak VL, Reddy VS, Prasad B, Nimbarte VD, Srinivasulu V, Vishunuvardhan MVPS, Reddy CS. Synthesis and biological evaluation of benzo[*b*]furans as inhibitors of tubulin polymerization and inducers of apoptosis. ChemMedChem. 2014; 9:117–128. [PubMed: 24203459]

(20). Romagnoli R, Baraldi PG, Sarkar T, Carrion MD, Cruz-Lopez O, Lopez-Cara C, Tolomeo M, Grimaudo S, Di Cristina A, Pipitone MR, Balzarini J, Gambari R, Lampronti I, Saletti R, Brancale A, Hamel E. Synthesis and biological evaluation of 2-(3′,4′,5′-trimethoxybenzoyl)-3-*N*,*N*-dimethylaminobenzo[*b*]furan derivatives as inhibitors of tubulin polymerization. Bioorg. Med. Chem. 2008; 16:8419–8426. [PubMed: 18755591]

(21). Romagnoli R, Baraldi PG, Lopez Cara C, Cruz-Lopez O, Carrion MD, Kimatrai Salvador M, Bermejo J, Estévez S, Estévez F, Balzarini J, Brancale A, Ricci A, Chen L, Gwan Kim J, Hamel

E. Synthesis and antitumor molecular mechanism of agents based on amino 2-(3′,4′,5′-trimethoxybenzoyl)-benzo[*b*]furan: inhibition of tubulin and induction of apoptosis. ChemMedChem. 2011; 6:1841–1853. [PubMed: 21805646]

(22). Flynn BL, Hamel E, Jung MK. One-pot synthesis of benzo[*b*]furan and indole inhibitors of tubulin polymerization. J. Med. Chem. 2002; 45:2670–2673. [PubMed: 12036378]

(23). Flynn BL, Gill GS, Grobelny DS, Chaplin JH, Paul D, Leske AF, Lavranos TC, Chalmers DK, Charman SA, Kostewicz E, Shackleford DM, Morizzi J, Hamel E, Jung MK, Kremmidiotis G. Discovery of 7-hydroxy-6-methoxy-2-methyl-3-(3,4,5-trimethoxybenzoyl)benzo[*b*]furan (BNC105), a tubulin polymerization inhibitor with potent antiproliferative and tumor vascular disrupting properties. J. Med. Chem. 2011; 54:6014–6027. [PubMed: 21774499]

(24). Kremmidiotis G, Leske AF, Lavranos TC, Beaumont D, Gasic J, Hall A, O'Callaghan M, Matthews CA, Flynn BL. BNC105: a novel tubulin polymerization inhibitor that selectively disrupts tumor vasculature and displays single-agent antitumor efficacy. Mol. Cancer Ther. 2010; 9:1562–1573. [PubMed: 20515948]

(25). Chaplin JH, Gill GS, Grobelny DW, Flynn BL, Kremmidiotis G. Substituted benzofurans, benzothiophenes, benzoselenophenes and indoles and their use as tubulin polymerization inhibitors. PCT Int. Appl. 2007 WO2007087684.

(26). Hamel E. Evaluation of antimitotic agents by quantitative comparisons of their effects on the polymerization of purified tubulin. Cell Biochem. Biophys. 2003; 38:1–21. [PubMed: 12663938]

(27). Bhattacharyya B, Panda D, Gupta S, Banerjee M. Antimitotic activity of colchicine and the structural basis for its interaction with tubulin. Med. Res. Rev. 2008; 28:155–183. [PubMed: 17464966]

(28). Verdier-Pinard P, Lai J-Y, Yoo H-D, Yu J, Marquez B, Nagle DG, Nambu M, White JD, Falck JR, Gerwick WH, Day BW, Hamel E. Structure-activity analysis of the interaction of curacin A, the potent colchicine site antimitotic agent, with tubulin and effects of analogs on the growth of MCF-7 breast cancer cells. Mol. Pharmacol. 1998; 53:62–76. [PubMed: 9443933]

(29). Massarotti A, Coluccia A, Silvestri R, Sorba G, Brancale A. The tubulin colchicine domain: a molecular modeling perspective. ChemMedChem. 2012; 7:33–42. [PubMed: 21990124]

(30). Clarke PR, Allan LA. Cell-cycle control in the face of damage—a matter of life or death. Trends Cell Biol. 2009; 19:89–98. [PubMed: 19168356]

(31)(a). Kiyokawa H, Ray D. In vivo roles of cdc25 phosphatases: biological insight into the anti-cancer therapeutic targets. Anti-Cancer Agents Med. Chem. 2008; 8:832–836.(b) Donzelli M, Draetta GF. Regulating mammalian checkpoints through Cdc25 inactivation. EMBO Rep. 2003; 4:671–677. [PubMed: 12835754]

(32). Vermes I, Haanen C, Steffens-Nakken H, Reutelingsperger C. A novel assay for apoptosis. Flow cytometric detection of phosphatidylserine expression on early apoptotic cells using fluorescein labelled annexin V. J. Immunol. Methods. 1995; 184:39–51. [PubMed: 7622868]

(33). Mollinedo F, Gajate C. Microtubules, microtubule-interfering agents and apoptosis. Apoptosis. 2003; 8:413–450. [PubMed: 12975575]

(34). Rovini A, Savry A, Braguer D, Carré M. Microtubule-targeted agents: when mitochondria become essential to chemotherapy. Biochim. Biophys. Acta. 2011; 1807:679–88. [PubMed: 21216222]

(35). Chiu WH, Luo SJ, Chen CL, Cheng JH, Hsieh CY, Wang CY, Huang WC, Su WC, Lin CF. Vinca alkaloids cause aberrant ROS-mediated JNK activation, Mcl-1 downregulation, DNA damage, mitochondrial dysfunction, and apoptosis in lung adenocarcinoma cells. Biochem. Pharmacol. 2012; 83:1159–1171. [PubMed: 22285910]

(36). Romagnoli R, Baraldi PG, Cruz-Lopez O, Lopez Cara C, Carrion MD, Brancale A, Ricci A, Hamel E, Bortolozzi R, Basso G, Viola G. Convergent synthesis and biological evaluation of 2-amino-4-(3′,4′,5′-trimethoxyphenyl)-5-aryl thiazoles as microtubule targeting agents. J. Med. Chem. 2011; 54:5144–5153. [PubMed: 21663319]

(37)(a). Cai J, Jones DP. Superoxide in apoptosis. Mitochondrial generation triggered by cytochrome *c* loss. J. Biol. Chem. 1998; 273:11401–11404. [PubMed: 9565547] (b) Nohl H, Gille L, Staniek K. Intracellular generation of reactive oxygen species by mitochondria. Biochem. Pharmacol. 2005; 69:719–723. [PubMed: 15710349]

(38). Soldani C, Scovassi A. Poly(ADP-ribose) polymerase cleavage during apoptosis: an update. Apoptosis. 2002; 74:321–328. [PubMed: 12101391]

(39)(a). Matson DR, Stukenberg PT. Spindle poisons and cell fate: a tale of two pathways. Mol. Interventions. 2011; 11:141–150.(b) Wertz IE, Kusam S, Lam C, Okamoto T, Sandoval W, Anderson DJ, Helgason E, Ernst JA, Eby M, Liu J, Belmont LD, Kaminker JS, O'Rourke KM, Pujara K, Kohli PB, Johnson AR, Chiu ML, Lill JR, Jackson PK, Fairbrother WJ, Seshagiri S, Ludlam MJ, Leong KG, Dueber EC, Maecker H, Huang DC, Dixit VM. Sensitivity to antitubulin chemotherapeutics is regulated by MCL1 and FBW7. Nature. 2011; 471:110–114. [PubMed: 21368834]

(40). Gasparotto V, Castagliuolo I, Chiarelotto G, Pezzi V, Montanaro D, Brun P, Palù G, Viola G, Ferlin MG. Synthesis and biological activity of 7-phenyl-6,9-dihydro-3*H*-pyrrolo[3,2-*f*]-quinolin-9-ones: a new class of antimitotic agents devoid of aromatase activity. J. Med. Chem. 2006; 49:1910–1915. [PubMed: 16539377]

(41). Bergers G, Benjamin LE. Tumorigenesis and the angiogenic switch. Nat. Rev. Cancer. 2003; 3:401–410. [PubMed: 12778130]

(42). Guidolin D, Vacca A, Nussdorfer GG, Ribatti D. A new image analysis method based on topological and fractal parameters to evaluate the angiostatic activity of docetaxel by using the Matrigel assay in vitro. Microvasc. Res. 2004; 67:117–124. [PubMed: 15020202]

(43). Porcù E, Viola G, Bortolozzi R, Mitola S, Ronca R, Presta M, Persano L, Romagnoli R, Baraldi PG, Basso G. TR-644 a novel potent tubulin binding agent induces impairment of endothelial cells function and inhibits angiogenesis. Angiogenesis. 2013; 16:647–662. [PubMed: 23456551]

(44). Ravelli RBG, Gigant B, Curmi PA, Jourdain I, Lachkar S, Sobel A, Knossow M. Insight into tubulin regulation from a complex with colchicine and a stathmin-like domain. Nature. 2004; 428:198–202. [PubMed: 15014504]

(45). Dorleans A, Gigant B, Ravelli RB, Mailliet P, Mikol V, Knossow M. Variations in the colchicine-binding domain provide insight into the structural switch of tubulin. Proc. Natl. Acad. Sci. U.S.A. 2009; 106:13775–13779. [PubMed: 19666559]

(46). Molecular Operating Environment (MOE). version 2008.10. Chemical Computing Group, Inc.; Montreal, Quebec, Canada: http://www.chemcomp.com

(47). Korb, O.; Stützle, T.; Exner, TE. PLANTS: Application of ant colony optimization to structure-based drug design. In: Dorigo, M.; Gambardella, LM.; Birattari, M.; Martinoli, A.; Poli, R.; Stützle, T., editors. Ant Colony Optimization and Swarm Intelligence, 5th International Workshop, ANTS 2006; Berlin: Springer; 2006. p. 247-258.LNCS 4150

(48). Pistollato F, Abbadi S, Rampazzo E, Viola G, Della Puppa A, Cavallini L, Frasson C, Persano L, Panchision DM, Basso G. Succinate and hypoxia antagonizes 2-deoxyglucose effects on glioblastoma. Biochem. Pharmacol. 2010; 80:1517–1527. [PubMed: 20705058]

(49). Liang CC, Park AY, Guan JL. In vitro scratch assay: a convenient and inexpensive method for analysis of cell migration in vitro. Nat. Protoc. 2007; 2:329–333. [PubMed: 17406593]

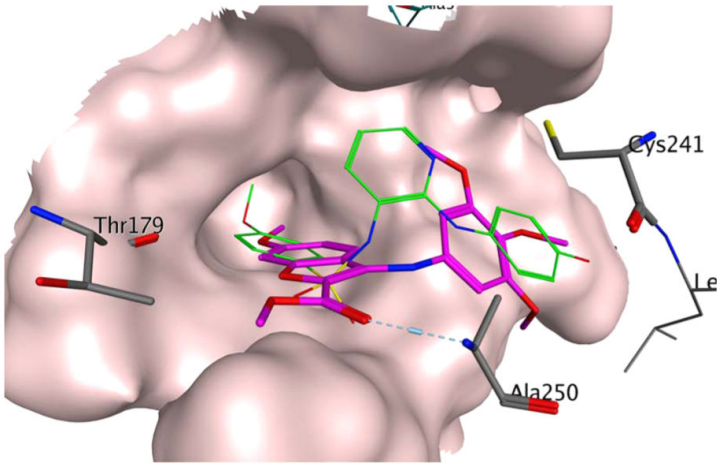

Figure 1.

Proposed binding of **3g** (represented in magenta) in the colchicine site of tubulin (PDB code 3HKC). The cocrystallized ligand *N*-[2-[(4-hydroxyphenyl)amino]-3-pyridinyl]-4-methoxybenzenesulfonamide (ABT751) is represented in green.

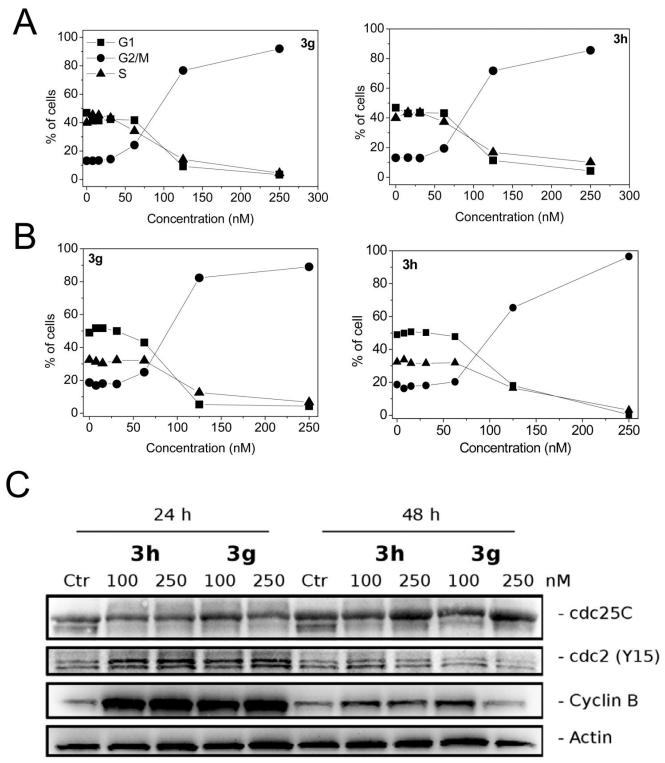

Figure 2.

Percentage of cells in each phase of the cell cycle in Jurkat (A) and HeLa (B) cells treated with **3g** or **3h** at the indicated concentrations for 24 h. Cells were fixed and labeled with PI and analyzed by flow cytometry as described in the Experimental Section. (C) Western blot analysis of some G2/M regulatory proteins after treatment with **3g** or **3h**. HeLa cells were treated for 24 or 48 h with the indicated concentration of compound. The cells were harvested and lysed for the detection of cyclin B, p-cdc2^{Y15}, and cdc25c expression. To confirm equal protein loading, each membrane was stripped and reprobed with anti-*β*-actin antibody.

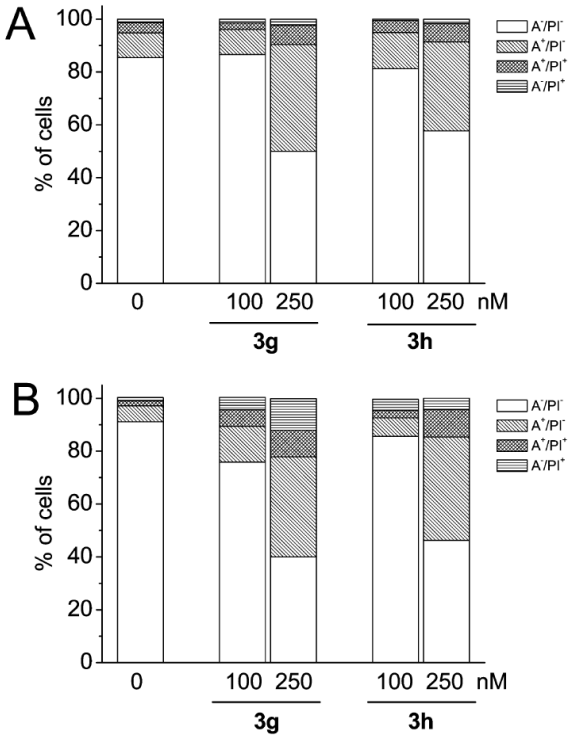

Figure 3.

Flow cytometric analysis of apoptotic cells after treatment of HeLa cells with **3g** or **3h** at the indicated concentrations after incubation for 24 (A) or 48 h (B). The cells were harvested and labeled with annexin-V-FITC and PI and analyzed by flow cytometry.

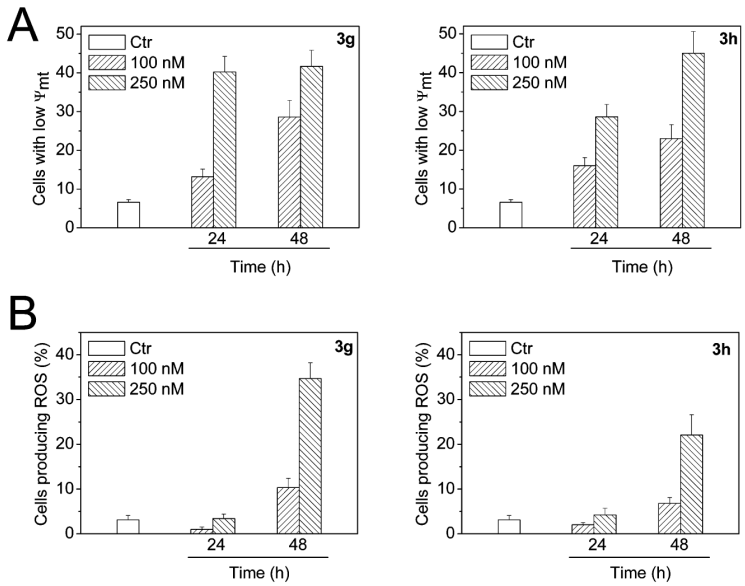

Figure 4.

(A) Assessment of mitochondrial membrane potential ($\Delta\psi_{mt}$) after treatment of HeLa cells with **3g** or **3h**. Cells were treated with the indicated concentration of compounds for 24 or 48 h and then stained with the fluorescent probe JC-1. Data are presented as the mean ± SEM of three independent experiments. (B) Mitochondrial production of ROS in HeLa cells following treatment with **3g** or **3h**. After 24 or 48 h incubations, cells were stained with H_2-DCFDA and analyzed by flow cytometry. Data are presented as the mean ± SEM of three independent experiments.

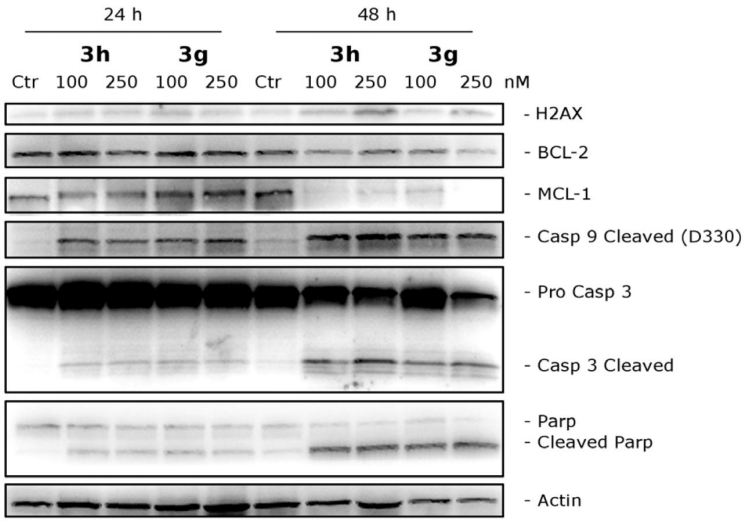

Figure 5.

Western blot analysis of H2AX, Bcl-2 Mcl-1, caspase-3, cleaved caspase-9, and PARP after treatment of HeLa cells with **3g** or **3h** at the indicated concentrations for the indicated times. To confirm equal protein loading, each membrane was stripped and reprobed with anti-β-actin antibody.

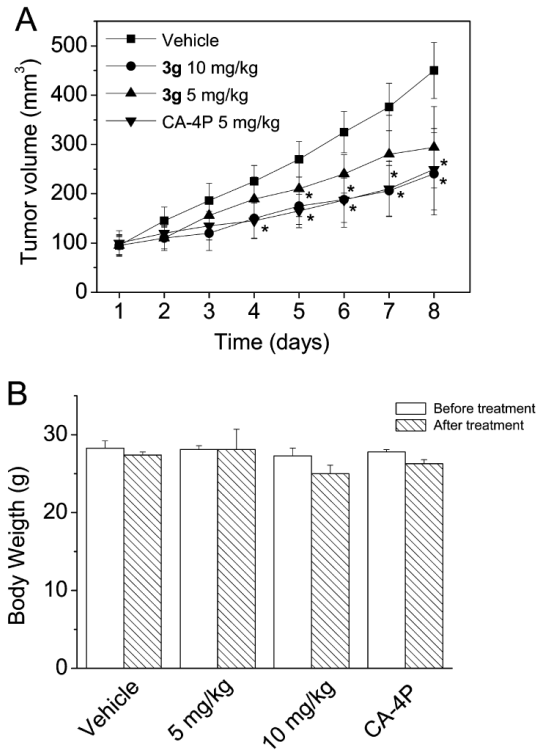

Figure 6.

Inhibition of mouse allograft growth in vivo by compound **3g**. (A) Male mice were injected subcutaneously at their dorsal region with 10^7 BNL 1MEA.7R.1 cells, a syngenic hepatocellular carcinoma cell line. Tumor-bearing mice were administered the vehicle, as control, or **3g** at a dose of 5 or 100 mg/kg or CA-4P (5 mg/kg) as reference compound. Injections were given intraperitoneally daily starting on day 1. The figure shows the average measured tumor volumes (A) and body weights of the mice (B) recorded at the beginning and at the end of the treatments. Data are presented as the mean ± SEM of tumor volume and body weight at each time point for 5 animals per group: (∗) $p < 0.01$, vs control.

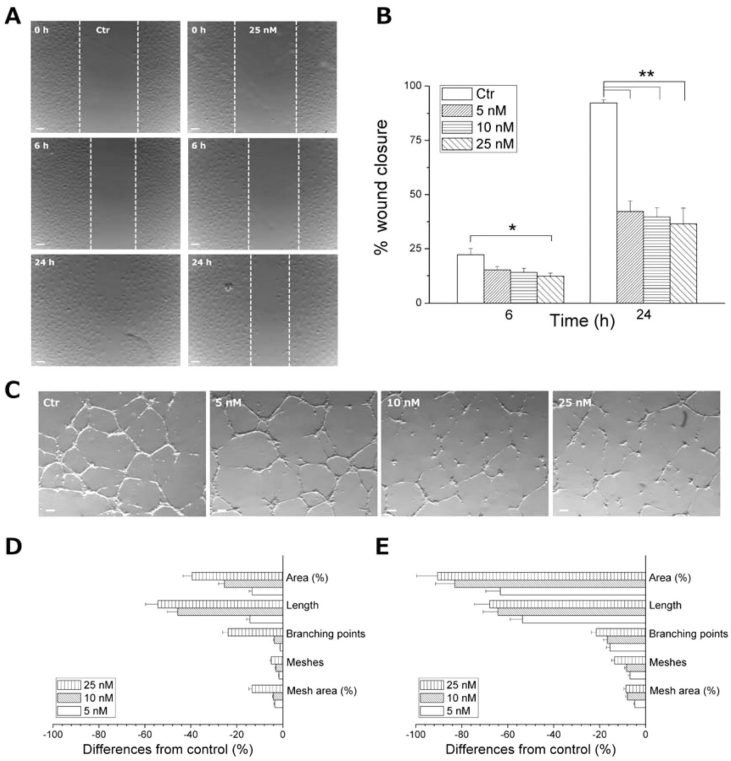

Figure 7.

Compound **3g** has antivascular activity in vitro. (A) Confluent HUVECs in a monolayer were wound, and cells were treated with different concentrations of **3g** and photographed at various times, 7× magnification; bar = 100 μm. The dotted lines define the areas lacking cells. (B) The graph shows the quantitative effect of **3g**. Migration was quantified by measuring the gap closure at the indicated times. Data are represented as the mean ± SEM of three independent experiments: (∗) $p < 0.05$, (∗∗) $p < 0.01$ vs control. (C) Inhibition of endothelial cell capillary-like tubule formation by **3g**: representative pictures (10× magnification; bar = 100 μm) of preformed capillary-like tubules treated with increasing concentration of **3g** for 1 or 3 h. (D, E) Quantitative analysis of the effects of **3g** on the dimensional and topological parameters of the preformed capillary-like tubule networks after a 1 h (D) or a 3 h treatment (E). Data are represented as the mean ± SEM of three independent experiments.

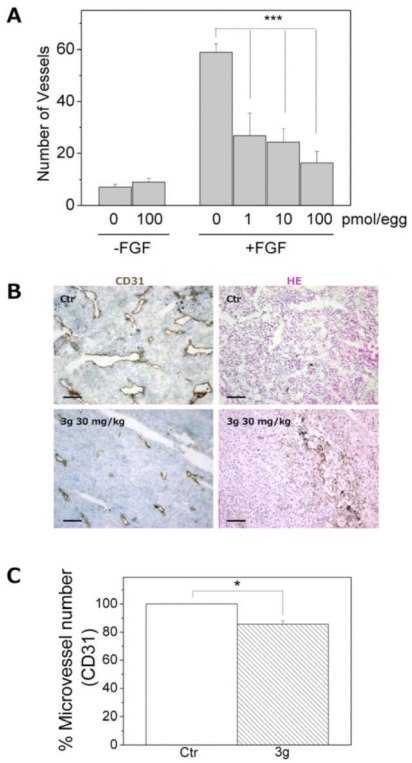

Figure 8.

In vivo effects of **3g** on angiogenesis. (A) CAM assay. Alginate sponges embedded with FGF, a stimulator of blood vessel formation, in the presence of the indicated concentrations of **3g** were implanted on the top of the growing CAM on day 11 of development. On day 14, newly formed blood vessels converging toward the implants were counted microscopically. Data represent the mean ± SEM of at least six eggs for each group: (∗∗∗) $p < 0.001$ vs control. (B, C) Efficacy in vivo of **3g** in a syngeneic mouse model. (B) BL6-B16 murine melanoma cells were injected in the right flank of C57BL/6 mice as described in the Experimental Section. Tumor tissues were embedded in OCT compound and frozen for immunohistochemistry: CD31 immunohistochemistry and hematoxylin–eosin (HE) staining of tumor after ip treatment with 30 mg/kg of **3g** (100× magnification). (C) Quantitative analysis of tumor section stained with CD31 for blood vessel number. Data are represented as the mean ± SEM of five mice per group: (∗) $P < 0.05$ versus control.

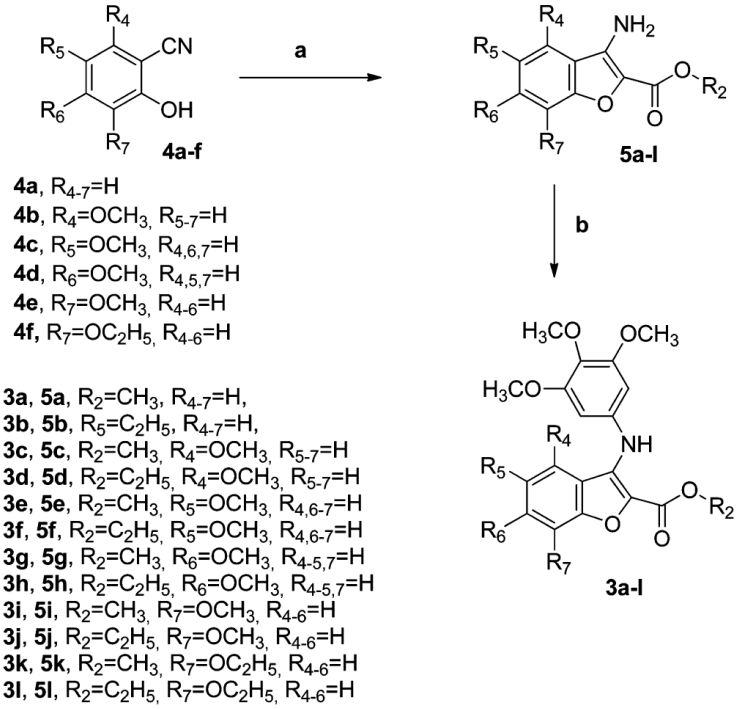

Scheme 1a.

[a]Reagents: (a) $BrCH_2CO_2CH_3$ or $BrCH_2CO_2C_2H_5$, K_2CO_3, DMF, 60 °C for 4 h then reflux for 8 h; (b) 1-bromo-3,4,5-trimethoxybenzene, $Pd(OAc)_2$, BINAP, Cs_2CO_3, PhMe, 100 °C, 16 h.

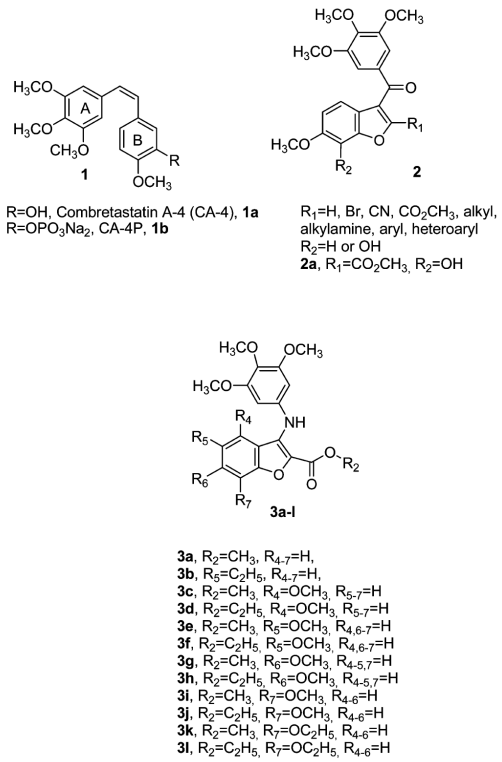

Chart 1.

Chemical Structures of CA-4 (1a), CA-4P (1b), 2-Substituted-3-(3,4,5-trimethoxybenzoyl)-6-methoxybenzo[*b*]furans 2, and 2-Alkoxycarbonyl-3-(3,4,5-trimethoxyanilino)benzo[*b*]furan Derivatives 3a–l

Table 1

In Vitro Cell Growth Inhibitory Effects of Compounds 3a–l and CA-4 (1)

	IC_{50}[a] (nM)						
compd	**HeLa**	**A549**	**HT-29**	**Jurkat**	**RS 4;11**	**MCF-7**	**HL-60**
3a	260 ± 50	5280 ± 800	930 ± 35	4100 ± 200	430 ± 97	7800 ± 900	4400 ± 200
3b	1330 ± 580	5470 ± 700	1600 ± 120	180 ± 38	300 ± 80	6600 ± 310	2500 ± 130
3c	>10000	>10000	>10000	>10000	>10000	>10000	>10000
3d	>10000	>10000	>10000	>10000	>10000	>10000	>10000
3e	250 ± 88	1570 ± 430	240 ± 60	210 ± 20	39 ± 9	7900 ± 1300	470 ± 30
3f	1260 ± 510	8900 ± 1460	1400 ± 540	2300 ± 700	190 ± 15	2900 ± 400	3400 ± 120
3g	2 ± 0.1	9 ± 1.4	3 ± 0.9	8 ± 0.6	0.3 ± 0.1	27 ±2	5± 1
3h	13 ±8	36 ± 11	17 ±8	22 ± 6	100 ± 10	25 ±3	24 ± 7
3i	130 ± 60	1270 ± 400	290 ± 30	30 ± 5	1± 0.1	520 ± 40	320 ± 17
3j	270 ± 80	1100 ± 300	110 ± 50	290 ± 50	230 ± 10	2100 ± 90	590 ± 50
3k	2530 ± 280	8900 ± 1300	3200 ± 210	3700 ± 450	400 ± 100	>10000	4200 ± 200
3l	3280 ± 370	7250 ± 237	5300 ± 290	9100 ± 820	3000 ± 400	>10000	5500 ± 540
CA-4	4 ± 1	180 ± 30	3100 ± 100	5 ± 0.6	0.8 ± 0.2	370 ± 100	1 ± 0.2

[a] IC_{50} = compound concentration required to inhibit tumor cell proliferation by 50%. Data are expressed as the mean ± SE from the dose–response curves of at least three independent experiments.

Table 2

Cytotoxicity of 3c and 3f in Human Noncancer Cells

	IC_{50} (μM)[a]	
cell line	**3g**	**3h**
$PBL_{resting}$[b]	>10	>10
PBL_{PHA}[c]	>10	6.3 ± 1.0
HUVEC	0.75 ± 0.4	0.22 ± 0.1

[a] Compound concentration required to reduce cell growth by 50%. Values are the mean ± SEM for three separate experiments.

[b] PBL not stimulated with PHA.

[c] PBL stimulated with PHA.

Table 3

Inhibition of Tubulin Polymerization and Colchicine Binding by Compounds 3e, 3g–j, and CA-4

compd	tubulin assembly[a] IC_{50} ± SD (μM)	colchicine binding[b] % inhibition ± SD
3e	7.5 ± 0.5	nd
3g	1.1 ± 0.1	83 ± 0.5
3h	1.5 ± 0.2	74 ± 4.1
3i	7.6 ± 1.0	nd
3j	6.4 ± 0.9	nd
CA-4 (**1a**)	1.1 ± 0.1	99 ± 0.1

[a] Inhibition of tubulin polymerization. Tubulin was at 10 μM.

[b] Inhibition of [^{3}H]colchicine binding. Tubulin, colchicine, and tested compound were at 1, 5, and 5 μM, respectively. nd: not determined.